Mineralogical and isotopic characterization of graphite deposits from the Anatectic Complex of Toledo, central Spain

Iván Martín-Méndez[1], Ester Boixereu[1], Carlos Villaseca[2]

[1]Instituto Geológico y Minero de España, Madrid, España, i.martin@igme.es, e.boixereu@igme.es
[2] Dpto. Petrología y Geoquímica, Facultad Geología, Instituto de Geociencias IGEO (UCM, CSIC), Madrid, España, granito@ucm.es

Corresponding author: Iván Martín Méndez, i.martin@igme.es

Abstract

Graphite is found dispersed in high-grade metapelitic rocks of the Anatectic Complex of Toledo (ACT) and was mined during the mid twentieth century in places where it has been concentrated (Guadamur and la Puebla de Montalbán mines). Some samples from these mines show variable but significant alteration intensity, reaching very low-T hydrothermal (supergene) conditions for some samples from the waste heap of the Guadamur site (<100 ºC and 1kbar). Micro-Raman and XRD data indicate that all the studied ACT graphite is of high crystallinity irrespectively of the degree of hydrothermal alteration. Chemical differences were obtained for graphite $\delta^{13}C$ composition. ACT granulitic graphite shows $\delta^{13}C_{PDB}$ values in the range of -20.5 to -27.8‰, indicating a biogenic origin. Interaction of graphite with hydrothermal fluids does not modify isotopic compositions even in the most transformed samples from mining sites. The different isotopic signatures of graphite from the mining sites reflect its contrasted primary carbon source. The high crystallinity of studied graphite makes this area of central Spain suitable for graphitic exploration and its potential exploitation, due to the low carbon content required for its viability and its strategic applications in advanced technologies, such as graphene synthesis.

Key words: Graphite, XRD, Raman spectra, carbon isotopes, Variscan granulites

Introduction

Graphite is primarily found in metamorphic rocks although it can appear in other geological settings. There are four common types of graphite in nature: i) graphite formed through metamorphism of biogenic carbonaceous material, ii) mantle-derived graphite, iii) graphite formed as precipitates from aqueous fluids and iv) graphite formed through reduction of carbonates (e.g., Luque et al. 1998; Galvez et al. 2013).

Graphite is considered a critical mineral due to its low abundance in nature and because it is a strategic material for the manufacturing of electronic devices, as lubricant, as a cathode for Li-ion batteries and is commonly used in nanotechnology. It is expected that the demand for graphite will increase approximately a 4% in the coming years (e.g., Lazzeri and Barreiro 2014).

Graphite deposits are scarce in the world. The main graphite deposits in the world are in metamorphic terrains like those in Orissa state in India and the Precambrian Granulitic Complex of Wanni in Sri Lanka (Luque et al. 2014), although there are other deposits in China, Brazil, Mexico and Madagascar (Beyssac and Rumble 2014). In Spain, the main deposits are in Málaga (Ronda peridotites, where graphite is associated with sulphides in ultramafic rocks) (Luque et al. 1992; Crespo et al. 2006a), Huelva (Almonaster la Real, Cortegana, Aroche and Santa Ana la Real, where graphite is present in high-grade metamorphic rocks) (Rodas et al. 2000; Crespo et al. 2004), Segovia (El Muyo, Madriguera, Becerril and Ayllón, where graphite and carbonaceous material are associated with black shales) (Barrenechea et al. 1991) and the Toledo anatectic complex (Luque et al. 1992; IGME 1995).

In this paper we document graphite occurrences within the "Anatectic Complex of Toledo" (ACT) which is located in the Central Iberian Zone of the Variscan Belt. Graphite is an accessory mineral present in most of the metasedimentary-derived rocks from this high-grade anatectic complex. Moreover, two graphite deposits that were previously mined in the twentieth century appear in this zone: the Guadamur and "La Española" (la Puebla de Montalbán) mines. Graphite in metasedimentary rocks usually has a biogenic origin and is formed by the change of organic carbonaceous material in sediments due to metamorphic processes (Buseck and Beyssac 2014). Graphite deposits are mainly

59 associated with high- and medium-grade metamorphic rocks like the granulite-facies rocks found in
60 the ACT. As graphite is not incorporated into the melt fraction of a partial melting process, is
61 considered a melting residue (e.g, Cesare and Maineri 1999). The amount of graphite in
62 metamorphosed metasedimentary rock depends greatly on the metamorphic degree and the melting
63 fraction underwent during anatexis in granulite-facies rocks.

64 The aim of this work is to characterize the graphite from granulitic rocks and from mined areas of
65 la Puebla de Montalbán and Guadamur sites and to compare the ordered and high temperature graphite
66 (in granulites) from the graphite that appears in more hydrothermally affected areas (in mines). In the
67 la Puebla de Montalbán area some graphite is locally concentrated along late micro shear bands. The
68 common association of graphite to highly deformed metamorphic rocks and the combined roles of
69 deformation processes and fluid percolation for graphite deposition during late stages of granulite
70 terrane exhumation are key factors in the study of ACT graphite deposits. Thus, we have analyzed the
71 graphite crystallinity using X-ray diffractometry (XRD) and micro-Raman spectroscopy. Carbon
72 isotopes have been performed to study the origin of the carbon sources and the possible role of
73 hydrothermal fluids in local graphite remobilization. Pressure-temperature conditions of graphite
74 crystallization and re-equilibration have been estimated from mineral paragenesis in each of the two
75 mined areas. To our knowledge this is the first study devoted to the ACT graphite from the first
76 graphite producing area in Spain, and probably its largest and most strategically important reservoir of
77 this ore due to its highly ordered structure.

78

79 **Geological setting**

80 The Anatectic Complex of Toledo (ACT) is located to the south of Toledo city and occupies an
81 area of around 100 km^2 (Fig. 1). The southern limit is defined by a mylonitic zone, a late-Variscan
82 ductile normal fault with listric geometry (Toledo shear zone). This fault separates the anatectic-
83 granulitic complex from Paleozoic to Neoproterozoic low grade metasedimentary rocks of the
84 southern *Schist Greywacke Complex* (Aparicio 1971; Barbero 1992; Barbero and Villaseca 2004). The

85 northern limit is delimitated by a set of E-W-trending alpine faults, that separate high grade rocks of
86 the ACT from Cenozoic sediments of the Tagus basin (Fig. 1).

87 The ACT is a high-grade metamorphic terrane located in the inner areas of the Central Iberian
88 Zone. The high-grade metamorphism of the ACT is of Variscan age (around 314 to 310 Ma, Barbero
89 and Rogers 1999 by monazite U-Pb dating; Castiñeiras et al. 2008 by zircon U-Pb dating). Three main
90 groups of rocks have been distinguished in the ACT (Barbero 1995; Barbero and Villaseca 2004) (Fig.
91 1): (1) High-grade metamorphic rocks of two types: (a) granulite-facies pelitic metasedimentary rocks
92 with complex migmatite structures, interlayered with semi-pelitic sediments and minor quartzites,
93 calc-silicate rocks and marbles; (b) orthogneisses of felsic composition, mainly augen-gneisses and
94 leucogneisses. (2) Highly to moderately peraluminous granitoids of anatectic character, ranging from
95 restite-rich varieties (e.g., Layos type, Barbero and Villaseca 1992) to anatectical leucogranites (e.g.,
96 Cervatos type, Barbero et al. 1995). Most of these peraluminous suites are interpreted as having been
97 generated during Variscan anatexis of ACT materials (Barbero 1992; Barbero et al. 1995). (3)
98 Intrusive calc-alkaline granitoids (Argés type) and associated basic rocks that were emplaced syn-
99 orogenically during the Variscan metamorphic climax and underwent the granulite-facies
100 migmatization.

101 The metamorphic peak conditions of the ACT were estimated to be 800 ± 50 ºC and 4-6 kbar
102 followed by a retrograde cooling recorded by garnet rim conditions at broader conditions of 600 to 700
103 ºC and below 3 kbar (Barbero, 1995). The study of non-aqueous fluid inclusions in ACT migmatites
104 indicates that at those mid-T conditions of 550 ºC, the ACT was exhumed to pressures below 1 kbar
105 (Martín Romera et al. 2001).

106 Peraluminous granulites and migmatites are the most abundant metamorphic rocks in the complex
107 and the main host of graphite in the ACT. The granulites can have migmatitic banding or massive
108 granoblastic texture and are interpreted as residual rocks after granite melt extraction (Barbero 1995;
109 Barbero et al. 1995). Graphite is a common accessory mineral in these residual granulites.

110 Two graphite-rich sectors in the ACT were mined: La Puebla de Montalbán (La Española
111 exploitation), and the Guadamur mine. The la Española and Guadamur mines were exploited berween

1939 and 1961, being the main producers of graphite in Spain at that time. The la Española graphite deposit is located to the north of Gálvez (Fig. 1), and was mined from 1943 to 1947, producing around 530 tonnes of graphite. In 1946 the mine was closed due to transport problems and the plant was moved to Guadamur (Sánchez Ronda 2013). The Guadamur mines were active until 1961 in two periods of time; the first from 1919 to 1920 when 310 tonnes of graphite was obtained, and the second from 1947 to 1961 producing 4500 tonnes). These graphite mines were the last ones exploited in Spain.

Some samples from Guadamur mines were boulders taken from tailing deposits and waste heaps as the underground excavations had collapsed and were covered for safety (samples 114432, 114433, 114434). Additional sampling was taken from trenches and neighbor areas. Samples from the La Puebla de Montalbán area were taken from the surroundings and local excavations. In the latter case some graphite-rich bands are concentrated by late extensional micro-shears with orientations of N110-40NE to N135-50NE (Fig. 2).

Analytical methods

Two types of graphite were sampled for this study: (1) granulitic graphite of the ACT and from one granulite xenolith from the lower crust of the Spanish Central System (SCS) in central Spain (sample U-10 from Villaseca et al. 1999), (2) graphite from the two mined sites.

Major-element mineral compositions were determined at the *Centro Nacional de Microscopía Electrónica "Luis Bru"* (Universidad Complutense de Madrid) using a Jeol JXA-8900 M electron microprobe with five wavelength dispersive spectrometers. Analytical conditions were an accelerating voltage of 15 kV and an electron beam current of 20 nA, with a beam diameter of 5 μm. Elements were counted for 10 s on the peak and 5 s on each background position. Corrections were made using the ZAF method. Analytical precision is 0.5-6 % for oxides with concentrations > 0.5 wt% whereas those with contents <0.5 wt% have uncertainties close to 10%. Results are reported in Table 1.

Graphite-rich samples from granulites and mining areas were analyzed using a Bruker D8 Advance X-ray diffractometer (DRX) at the *CAI Técnicas Geológicas* of the Universidad

Complutense of Madrid with Cu$K\alpha$ (40kV, 40mA) radiation. The 2θ values of the obtained peaks were calibrated using an internal corundum standard. The thickness of Lc(002) was calculated using the Scherrer equation (Scherrer 1918) . DRX were also used for volumetric analysis (wt% of C) and semiquantitative mineral estimation. Data processing was performed using DIFFRAC.Suite Eva software (https://www.bruker.com/es/products/x-ray-diffraction-and-elemental-analysis/x-ray-diffraction/xrd-software/overview/eva.html). Samples analysed and results are reported in Table 2.

A concentrated carbon-rich fraction of samples from mining areas was prepared in the IGME laboratories, at Tres Cantos (Madrid), before submitting to isotope analyses. This was done using HCl and HF acid dissolution to remove silicate and carbonate minerals. In addition, graphite from granulite samples was separated using standard mineral separation techniques and handpicking. Carbon stable isotope analyses of graphite were done in the Stable Isotope Laboratories of the University of Salamanca. The determination of isotope $^{13}C/^{12}C$ ratios in graphite was performed by combustion in an elemental analyzer EA3000 Eurovector coupled online to a mass spectrometer Isoprime (TM) in "continuous flow". The results (the mean value of triplicate analysis ± 1 standard deviation) are reported in δ ‰ relative to the PDB standard for carbon. Laboratory machine standard CO_2 gas measurements gave reproducibility better than 0.1 ‰.

Micro-Raman analyses were done in the laboratories of the Museo Nacional de Ciencias Naturales de Madrid (CSIC). Raman spectra were collected on unpolished rock chip surfaces to avoid damage from polishing (e.g., Pasteris 1989; Beyssac et al. 2003). A 532 nm wavelength beam from a 5-10 mW laser was focused on Thermo Fischer CRX microscope using 50x or 100x objectives for the analysis. Under these conditions the spectral resolution was 2-4 cm^{-1} and the spectral range was 100-2900 cm^{-1}. The laser beam size was approximately 2 microns. Integration times were between 10 and 16 seconds for each acquisition. The final spectrum and mean value for each sample were obtained by summing 3 to 5 spectra acquired under the same operating conditions. No significant changes were observed in the second order Raman region of graphite, and thus the study focused on the first order Raman spectra (1100–1800 cm^{-1}). Data processing was performed by LabSpec software v.5.33.14, obtaining parameters derived from each spectrum by deconvoluting gaussian-lorentzian peaks.

Mineralogy of graphite samples

Graphite is mostly disseminated in the ACT samples, and its exploitation was focused in granulitic bands showing anomalous concentration of graphite-rich flakes. Graphite is an accessory mineral in the granulites, and is normally associated to biotite or other high-grade metamorphic minerals as garnet, sillimanite, cordierite, plagioclase, quartz or K-feldspar (Fig. 3a,b). Biotite is observed in granulites next to the mines associated to graphite. The composition of biotite crystals is similar to samples analyzed by Barbero et al. (1992) (Table 1). The modal amount of graphite is usually low in the high-grade metasedimentary rocks of the ACT, either in migmatites or as residual granulites (< 0.5 %), but in areas close to both mining sites some granulite-facies rocks with graphite-rich cm-size bands can reach concentrations up to 23 vol.% (Table 2) (Fig. 2).

In mining areas (at least in the best outcropping mine of the La Puebla de Montalbán) most of the exploited graphite was related to granulitic graphite-rich bands, whereas minor amount of graphite was extracted from late micro-shear bands associated to retrograded muscovite. Samples from the Guadamur site were more altered and original field relationships are more difficult to establish due to poor outcropping conditions. In all samples shape of graphite is flaky and is forming small lamellae between the phyllosilicates. The coarsest flakes are those from granulites (up to 450 μm), whereas it is around 150-250 μm in some Guadamur rubble (tailing) samples (Fig. 3f).

In the Guadamur mining zones muscovite is the most abundant mica clearly suggesting retrograde conditions. Most of the granulitic minerals are retrograded except quartz and some biotite not completely transformed to chlorite. Muscovite and chlorite crystals are usually associated with disseminated graphite suggesting local pseudomorphosis of pre-existing biotite and total feldspar retrogression by water-rich metasomatism (Fig. 3c,d).

Chlorites appear only in some of the Guadamur samples (Fig. 3d) (Table 2), indicating more intense retrogradation conditions than in the La Puebla de Montalbán area. It appears as interlayered flakes associated with graphite suggesting total transformation of previous micas (granulitic biotite

191 and secondary muscovite). Chemically they are ripidiolite to picnoclhorite (Table 1). In one sample
192 from Guadamur (114432) an extremely low-grade mineral paragenesis associated to graphite and
193 quartz was found: this is formed by kaolinite-goethite-jarosite. Kaolinite is found only in this waste
194 heap sample associated to black and metallic luster flakes of graphite, showing that graphite-rich
195 samples from Guadamur have been more retrograded than those from La Puebla de Montalbán mines
196 (Fig. 3e). Jarosite is the only sulfate found in Guadamur samples. Jarosite is associated with goethite
197 forming oxidation bands in that sample (Fig. 3f). This sulfate is formed at very low temperature,
198 around 100 ºC, by supergene alteration (Peters 2011). Moreover, Fe-rich hydroxides are abundant in
199 samples from Guadamur area suggesting significant either supergene or hydrothermal fluid alteration.
200 Goethite, the more abundant hydroxide, appears forming alternating bands with jarosite in rubble
201 samples. Associated to goethite another Fe-hydroxide rich in Si and Al, which might be chamosite
202 (James 1966) was also present in some samples (Fig. 3g) (Table 1).

203 Calcite was found in the two mining areas in hydrothermally retrograded samples, usually forming
204 veins or brecciated rocks. In all cases, carbonate appears in two scenarios: (1) forming intrusive small
205 veins or a network of veinlettes (Fig. 3h,i), never related to graphite flakes, (2) as brecciated rocks
206 with calcite cement within granulitic (variably transformed) fragments (Fig. 3g), always indicating that
207 carbonate percolation is a later hydrothermal stage. In Guadamur area, calcite is forming veins with
208 accessory aragonite in zoned vugs (geodes) (Fig. 3i).

209 Samples from Guadamur contain ilmenite crystals with alteration rims to anatase (Table 1 sample
210 114434). On the other hand, samples from La Puebla de Montalbán contain ilmenite partially
211 transformed to a titanium oxide with significant contents of SiO_2 (up to 23 wt%) and Al_2O_3 (23 wt%)
212 (Table 1), that could be pseudorutile (Fig. 3j). Pseudorutile is commonly originated by ilmenite
213 alteration and can also be variably hydroxylated (up to 10-12 wt% H_2O) (Grey and Li 2003). The most
214 transformed ilmenites are hydroxylated pseudorutiles (HSR phases) with low FeO and high H_2O
215 contents (up to 25 wt%) (Table 1). These data suggest that granulitic ilmenite have been variably
216 altered by hydrothermal fluid circulation in the samples from ACT mined areas. The most
217 hydroxylated pseudorutiles suggest hydrothermal low temperature conditions (150-260 ºC) as

218 described by Grey et al. (1983). Accessory pyrite could appear in some granulites, usually transformed
219 to hematite when retrograded.

220 In summary, ACT graphite is associated to minerals formed in three growth stages: (1) a primary
221 stage in while the graphite accompanies anhydrous granulitic minerals, (2) a retrograde stage in which
222 graphite is associated with hydrous minerals such as muscovite and chlorite, and (3) an
223 oxide/weathering stage in which the graphite is associated with jarosite, goethite and kaolinite (mainly
224 restricted to waste heap samples from Guadamur site).

225

226 **Graphite characterization**

227 *XRD and micro-Raman spectroscopy*

228 To obtain high quality data of graphite from XRD studies is very difficult due to the low
229 absorption coefficient of carbon. This problem can lead to errors associated to the displacement of the
230 main peak of the spectrum. To obtain better results, this survey focused on the analysis of the 002
231 peak, that shows the greatest intensity in well ordered graphite (Baiju et al. 2005). Moreover, carbon
232 contents were firstly determined in samples without chemical pre-concentration treatment (Table 2).
233 The data confirms that Guadamur samples have slightly more carbon (or graphite) contents (up to 24
234 wt%) than those from La Puebla de Montalbán (up to 20 wt%).

235 The full-width of the peak at half maximum values and d and 2θ position were estimated from
236 the diffractogram (Baiju et al. 2005). The crystal size (Lc) along stacking direction (Table 2) is
237 calculated from the next equation:

238 $$Lc_{(002)} = k\lambda/\beta_{(002)} \cos\theta$$

239 Where k is the shape constant (0.94), $\beta_{(002)}$ is the full width of the peak at half-maximum in
240 radian and λ is the X-ray wavelength in angstroms (1.5406). and θ is the angle of diffraction in
241 radians. The high Lc(002) values found in all ACT samples (> 800) suggest a highly crystalline
242 graphite phase irrespectively of its association to high-T or low-T phyllosilicates (Table 2).

Similarly, the Raman spectrum of graphite is very sensitive to changes in crystallinity (e.g., Pasteris and Wotapenka 1991; Wotapenka and Pasteris 1993).There are two main regions of interest in graphite Raman spectrum. The first one occurs between 1100 and 1800 cm^{-1} and the second one between 2500 and 3100 cm^{-1}, called the first order spectrum and second order spectrum, respectively (Cesare and Maineri 1999; Beyssac et al. 2002). The most important characteristics in graphite Raman spectrum are: the G peak that appears approximately at 1580 cm^{-1} (ordered graphite), the D and D_0 peaks around 1350 and 1620 cm^{-1} (disordered graphite) and the S peak around 2700 cm^{-1} (Beyssac and Lazzeri 2012).

Raman spectra of samples collected from late retrograded micro-shears in Galvez area show a G peak in a position around 1580 cm^{-1} with a significant height difference with the D peak, around 1350 cm^{-1} (Fig. 4). This height difference (R2 values in Table 2) has been usually interpreted as a reflection of high ordered graphite. Spectra from U-10 and ACT granulites are very similar to those of La Puebla de Montalbán (Table 2). Graphite from Guadamur samples show spectra identical to the previously described. In these spectra the G peak is very pronounced and a small D peak appears in some determinations as typically found in highly ordered graphite (Cesare and Maineri 1999). Moreover, graphite spectra obtained from the Guadamur sample with kaolinite and jarosite, is also similar to the other ACT samples due to the high crystallinity of this phase, clearly not structurally affected by hydrothermal fluid circulation (Fig. 4).

Carbon isotopic composition

Graphite appears disseminated in different ACT rocks: (a) as an accessory mineral in granulites, (b) concentrated in local cm-size bands in granulites in the surroundings of the mining areas, (c) in strongly hydrothermally altered rocks, locally with carbonate veined samples or breccias, in the Guadamur mining area. To evaluate the evolution pattern of isotopic composition and a possible source of carbon we have analyzed the $\delta^{13}C$ of samples from the different areas described above, as well as in a UHT granulitic xenolith from the lower crust of the neighbor Spanish Central System (U-10 granulite of Villaseca et al. 1999). There are three potentials sources of carbon: (1) devolatilization

of carbonaceous metapelites, (2) mantle-derived and (3) decarbonation of carbonate rocks (e.g., Luque et al. 1998; Barrenechea et al. 2009).

Three different graphite types in the ACT were clearly distinguished on the basis of the carbon isotope results (Table 2). (1) the values of $\delta^{13}C_{PDB}$ of -18.3 to -19.7 ‰, obtained from U-10 sample, indicate an organic origin of carbon. Carbon isotope values from the ACT granulites define a wide range between -20.5 to -27.8‰, also indicating a biogenic carbon source. The highest ACT values are close to those of the lower crustal granulites from central Spain, in spite of the difference in P-T metamorphic conditions (Fig. 5). Values from graphite-rich a granulites from La Puebla de Montalbán range from -20.5 to -23.4‰, a range of values that include those found in samples from the neighbor mining site (-23.0 to -23.2‰, Table 2). Finally, a restricted range of $\delta^{13}C_{PDB}$ (-27.6 to -27.9 ‰, Table 2) indicates that Guadamur mining site samples have the lowest carbon isotope values, although such ligth values are also found in regional granulitic material (Table 2). In summary, graphite samples from mining areas show a remarkable narrow isotopic compositional range that, nevertheless, is always found in the surrounding granulitic rocks. A carbonate sample from an intrusive vein in strongly hydrothermalized rocks of the Guadamur site yields a $\delta^{13}C_{PDB}$ value of -5.15 (Table 2), in the typical range of carbonates (e.g., Luque et al. 2012), and similar to values found in hydrothermal carbonates of the Neoproterozoic metamorphic series of central Spain (Herrero et al. 2011).

Discussion

Thermometric estimation of retrograded graphite-rich samples based on mineral paragenesis

P-T estimations of retrograded ACT samples have been mainly achieved by paragenetic relations between graphite and surrounding phyllosilicates, mainly biotite, muscovite, chlorite and kaolinite (Fig. 6).

As previously described, the ACT underwent a metamorphic peak around 800 ± 50 ºC and 4-6 kbar and later suffered a retrogradation event with temperature below 700 ºC and pressure decreasing to 2 kbar (data obtained from P-T estimations using garnet rims) (Barbero 1995) (Fig. 6). Furthermore,

296 data obtained in fluid inclusions in quartz from granulites show a later exhumation stage in the ACT,
297 to pressures lower than 1 kbar and temperatures around 600 ºC for the highest-T carbonic inclusions
298 (Martín Romera et al. 2001). This fluid inclusions study describes an evolution from CO_2-rich fluids
299 (close to post-peak conditions) towards mixed CO_2-N_2-CH_4-rich fluids, and later low temperature non-
300 aqueous N_2-CH_4-rich inclusions associated to aqueous fluid inclusions (at <200 ºC). The presence of
301 common accessory graphite within the granulite matrix suggests that it was equilibrated during
302 granulite metamorphism at very low volatile conditions (Barbero 1995).

303 Low-temperature minerals associated to graphite observed in this study allow us to define
304 three different retrograde stages (Fig. 6). The first one is related to the muscovite recrystallization at
305 around 500 ºC, the second stage could be related to the occurrence of chlorite, around 400 ºC, and the
306 third stage explain the occurrence of kaolinite at temperatures below 300 ºC probably of supergene
307 conditions and related to surface weathering (Fig. 6). These three stages experienced very little
308 variations of pressure, (i.e., ≤ 1 kbar), according to data from fluid inclusions (Martín Romera et al.
309 2001).

310 Different *P-T* conditions derived by paragenetic assemblages were observed by comparing La
311 Puebla de Montalbán and Guadamur graphite-rich samples. La Puebla de Montalbán graphite-bearing
312 samples may have biotite or biotite plus muscovite (Fig. 6 stage 1), whereas in the Guadamur samples
313 graphite is associated with muscovite, chlorite and also kaolinite. Moreover, jarosite was only found in
314 the kaolinite-bearing sample from Guadamur, which is a supergene alteration mineral formed near to
315 surface, indicating the most recent alteration with temperatures <100 ºC. We can conclude that
316 temperatures recorded by retrograded phyllosilicate formation from La Puebla de Montalbán are
317 higher than those from Guadamur area (Fig. 6 stages 2 and 3).

318 Graphite formed at granulitic conditions interacted with hydrothermal fluids when the
319 granulitic high-T minerals were completely transformed to new low-T and H_2O-rich phases, being this
320 retrogradation more effective in local micro-domains (late shear bands or brittle vein systems)
321 occurring in studied mining areas. Nevertheless, the refractive character of graphite permits the

conservation of its high crystallinity also maintaining its chemical composition due to the sluggish diffusion kinetics of graphite with fluids (Wada 1988), as will be discussed below.

High crystallinity of the ACT graphite

The accessory graphite found in the studied high-T granulites of central Spain is highly crystalline. Estimated temperature of granulite formation range from circa 1000 ºC in central Spain lower crustal granulitic xenoliths (e.g., Orejana et al. 2010) to 800 ºC in the ACT granulite terrane (Barbero 1995). Graphite with full-ordered structure mostly appears in granulite rocks formed at > 700 ºC (e.g., Pasteris and Wopenka 1991; Baiju et al. 2005). The graphite of the lower crustal xenolith U-10 has Raman R2 ratios of 0.11 and XRD d(002) values (3.354, Table 2), typical of high grade metamorphic graphite (e.g., Shengelia et al. 1979; Wopenka and Pasteris 1993; Beyssac et al. 2002). Similarly, ACT granulites have graphite with R2 and d(002) values of 0.08 to 0.12 and 3.354 to 3.365, respectively (Table 2). Sample 114568 from La Puebla de Montalbán, which is affected by a microshear band (Fig. 2b), has, unexpectedly, the lowest crystallinity values of the whole data set (Table 2), with lower Raman and XRD parameters than those found in pervasively hydrothermallized and mylonitized samples from ACT mining areas. Nevertheless, graphite from this granulite is in the range of well-ordered structural features.

The graphite from the strongly hydrothermalized samples from the Guadamur mines has the same high degree of crystallinity when compared with the graphite in the nearby granulite rocks (Table 2). This is shown by comparing the Raman parameter R1 (Intensity $_{D\ band}$/Intensity $_{G\ band}$) in Guadamur graphite that range from 0.001 to 0.10 whereas the G band FWHM changes broadening from 15.06 to 16.07 (Table 2). Moreover, most Raman spectra have a humped S peak around 2700 cm^{-1} (Fig. 4), typical of high-T graphite (e.g., Beyssac et al. 2002). Using XRD data, the Lc(002) of the graphite varies from 879 to 1200 Å (Table 2) typical of high crystallinity (e.g., Shengelia et al. 1979; Baiju et al. 2005; Nakamura et al. 2014).

Some of the ACT graphite is affected by retrograded late micro-shear bands (mainly in the La Puebla de Montalbán mining area), but there is no evidence of significant graphite concentration with deformation, as those samples that have low modal graphite (2.2 to 7.8 wt%, samples 114554 to 114558 in Table 2) are clearly shifted to the lower part of the range of modal graphite within disseminated flakes in the surrounding granulites (1.5 to 20.1 wt%, Table 2). Moreover, the graphite in micro shear bands of La Puebla de Montalbán mine has the same well-ordered structure as the associated granulites without size reduction. This suggests that graphite structure during deformation towards low-T conditions in both mining areas of the ACT terrane was not associated with a lowering in crystallinity when compared to other granulitic areas. A simple explanation could be that graphite concentration in the ACT deposits is locally controlled by physical remobilization of pre-existing disseminated graphite and is not related to precipitation from hydrothermal fluids. Moreover, graphite related to these strongly hydrothermallized areas is not isotopically modified respect to the original granulitic graphite, as will be discussed in the next section.

The high crystallinity of studied graphite makes central Spain graphite suitable for applications in advanced technologies, as graphene synthesis. A previous work on metamorphic graphite in central Spain, on rocks from the eastern Spanish Central System, yielded Raman features of low crystallinity (R2 values of 0.8 or higher, Table 1 of Crespo et al. 2005) suggesting that only in high-grade areas (at granulite-facies conditions) rich in metasedimentary rocks of pelitic derivation, as those occurring at the studied ACT, are the most strategic areas for graphite exploration and exploitation for commercial viability (e.g., Beyssac and Rumble 2014).

Source of carbon

Isotopic $\delta^{13}C$ data are normally used to determine the source of carbon within the three main crustal existing reservoirs, which are characterized by different isotopic $\delta^{13}C$ values. Carbon from organic material ranges from -20 to -30‰, whereas carbon from carbonated sources has values close to 0‰. In contrast, carbon from mantle sources has values around -7 ‰ (e.g., Sanyal et al. 2009;

372 Touzain et al. 2010). As samples from this study have values between -20 and -30‰, we infer that
373 carbon in the ACT rocks has an organic origin.

374 Isotopic data from high-temperature granulites of the area (i.e., U-10 sample with $\delta^{13}C$ values
375 around -19‰ and ACT granulites around -20.5 to -27.8‰ (Table 2)), are indicative of the original
376 graphite, as these samples were not significantly affected by alteration or hydrothermal fluids. The
377 high variability in $\delta^{13}C$ signatures of the ACT granulites is representative of the carbon isotopic
378 heterogeneity of the primary organic material trapped in the original metasediments.

379 Carbon isotopic composition from samples of mining sites are quite different between them
380 but showing very uniform values within each deposit site (-23.1‰ ± 0.1 in the La Puebla de
381 Montalbán, and -27.6‰ ± 0.2 in Guadamur mines), values that are also found in the wide range of
382 $\delta^{13}C$ signatures of the surrounding granulites. Moreover, the remarkable homogeneity of carbon
383 isotope values of samples in each ACT mine suggest a lack of open system evolution during their
384 hydrothermal alteration and suggest the absence of significant chemical fractionation during fluid
385 interaction. Because of the retrograded low temperature conditions, the activation energy might not
386 have crossed the threshold necessary to precipitate the graphite or to trigger carbon isotope exchange
387 with percolating fluids. The carbon isotopic data implies a refractory character of the ACT graphite.
388 The deformed and retrograded graphite in the mining sites was not formed by precipitation from fluids
389 and was not chemically modified within the hydrothermal veining, and instead the results point just to
390 the physical remobilization of graphite during later retrograde events. The graphite in the mining areas
391 was converted from well-structured graphite into small fractured graphite (e.g., Fig. 3g), with its
392 carbon isotopic composition unchanged.

393 The absence of heavy $\delta^{13}C$ isotope values in the ACT samples is indicative of the absence of a
394 fluid precipitated origin for the graphite, and also indicates the lack of interaction with later carbonate
395 fluids, which show much heavier carbon isotope composition (-5.2‰, Table 2). The uniform $\delta^{13}C$
396 values of samples from ACT mines is indicative that retrograding and weathering processes have not
397 had a significant effect on their isotopic characteristics.
398

According to Manning et al. (2013), graphite precipitates with greater abundance at lower pressures, and in similar pressure conditions at higher temperatures. This could take place during peak and post-peak metamorphic conditions when the ACT was mainly exhumed to low pressure conditions (Barbero, 1992). The decompression of the ACT and its slow cooling, combined with natural deformation and fluid circulation focused in late micro-shears or hydrothermal veins were factors that failed to induce any chemical change of the ACT graphite or its recrystallization towards lower crystallinity types (or amorphous varieties of smaller size). General features of the granulitic graphite were maintained irrespectively of their alteration degree or mechanical deformation. This refractory character increases the resources and possibilities of mining and production of the ACT graphite for future processing and uses.

Conclusions

Graphite is found dispersed in many of the ACT rocks but it was mined in places where a greater concentration of black flakes appeared (Guadamur and La Puebla de Montalbán mines). In these mine pits, graphite was locally concentrated within late shear bands.

Micro-Raman and XRD data allow us to establish that all the studied ACT graphite is of high crystallinity irrespective of the hydrothermal degree of alteration of the sample. Thus, the ACT graphite is of high-temperature and refractory to structural changes during low-T fluid interaction. A trend in retrogradation conditions was observed in our study, reaching very low-T hydrothermal conditions some of the waste heap samples from the Guadamur mine site (<100 ºC and 1 kbar). The maintenance of high crystallinity in all studied samples indicates that graphite concentration in the ACT deposits is controlled by physical remobilization of pre-existing disseminated graphite and is not related to precipitation from hydrothermal fluids.

Chemical differences were obtained for graphite $\delta^{13}C$ composition. ACT granulites show $\delta^{13}C_{PDB}$ values between -20.5 to -27.8‰ reflecting the primary carbon isotopic heterogeneity of the organic material. $\delta^{13}C$ constant values have been found in samples from both mining sites (-23.1‰ ±

0.1 in the La Puebla de Montalbán, and -27.6‰ ± 0.2 in Guadamur), overlapping the wide range of $\delta^{13}C$ signatures of the surrounding granulites. This suggests a lack of carbon isotope exchange with hydrothermal fluids. Thus, graphite in the mining sites was not formed by precipitation from fluids but was physically remobilized during later retrograde events. This graphite was converted from well-structured graphite into small fractured graphite, with its carbon isotopic composition unchanged.

The high crystallinity of studied graphite makes ACT graphite suitable for exploration and exploitation, due to the low carbon content required for its commercial viability and strategic applications in advanced technologies, as graphene synthesis.

Acknowledgements

We acknowledge Alfredo Fernández Larios for his assistance with the electron microprobe analyses in the Centro Nacional de Microscopía Electrónica (UCM), and to Alberto Jorge García for his micro-Raman assistance in the Museo de Ciencias Naturales (CSIC). We also thanks to Xavier Arroyo Rey (CAI-DRX-UCM), and Jesús Reyes and Begoña del Moral from the analytical laboratories of the IGME their technical assistance. We thanks also to Jesús López Jerez for offering his sampling of granulites and graphite-rich rocks around mining areas of the ACT. We would like to especially thank Maite García Vallés for her assistance in Raman data processing. We also thank to Clemente Recio for his diligence in performing C isotope analyses in the Stable Isotope Laboratory of the Salamanca University. This work is included in the objectives of, and supported by, the CGL2012-32822 project of the Ministerio de Economía y Competitividad of Spain, and the 910492-UCM group. Finally, this study will be included in the metallogenetic database of the IGME.

References

Aparicio A (1971) Estudio geológico del Macizo Cristalino de Toledo. Est Geol 27: 361-414.

449 Baiju KR, Satish-Kumar M, Kagi H, Nambiar CG, Ravinsankar M. (2005) Mineralogical characterization of
450 graphite deposits from Thodupuzha-Kanjirappally Belt, Madurai Granulite Block, Southern India. Gond
451 Res 8: 223-230.

452 Barbero L (1992) Plutonismo sin-orogénico en un área granulítica Hercínica: El Complejo Anatéctico de Toledo.
453 Doctoral dissertation. University Complutense of Madrid

454 Barbero L (1995) Granulite-facies metamorphism in the Anatectic Complex of Toledo, Spain: late Hercynian
455 tectonic evolution by crustal extension. J Geol Soc London 152: 365-382.

456 Barbero L, Rogers G (1999) Implications of U-Pb monazite ages from synorogenic granites of the anatectic
457 complex of Toledo (Spain) in the evolution of the central part of the Hercynian Iberian Belt. Doc BRGM
458 290: 203.

459 Barbero L, Villaseca C (1992) The Layos granite, Hercynian Complex of Toledo (Spain): an example of
460 parautochthonous restite-rich granite in a granulitic area. Trans Roy Soc Edinburgh: Earth Sci 83: 127-138.

461 Barbero L, Villaseca C, Rogers G, Brown P (1995) Geochemical and isotopic disequilibrium in crustal melting:
462 An insight from the anatectic granitoids from Toledo, Spain. J Geoph Res 100: 15745-15765.

463 Barbero L, Villaseca C (2004) El macizo de Toledo. In: Vera JA (ed) Geología de Geología de España, SGE-
464 IGME, Madrid, pp 110-115.

465 Barrenechea JF, Luque FJ, Millward D, Ortega L, Beyssac O, Rodas M (2009) Graphite morphologies from the
466 Borrowdale deposit (NW England, UK): Raman and SIMS data. Contr Mineral Petrol 158: 37-51.

467 Beyssac O, Coffé B, Chopin C, Rouzaud J N (2002) Raman spectra of carbonaceous material in metasediments:
468 a new geothermometer. J Metam Geol 20: 859-871.

469 Beyssac O, Goffé B, Petitet JP, Froigneux E, Moreau M, Rouzaud JN (2003) On the characterization of
470 disordered and heterogeneous carbonaceous materials by Raman spectroscopy. Spectrochimica acta part A:
471 Molecular and biomolecular spectroscopy 59: 2267-2276.

472 Beyssac O, Lazzeri M (2012) Application of raman spectroscopy to the study of graphitic carbons in the earth
473 sciences. European Mineralogical Union Notes in Mineralogy 12: 451-454.

474 Beyssac O, Rumble D (2014) Graphitic carbon: a ubiquitous, diverse, and useful geomaterial. Elements 10: 415-
475 420.

476 Buseck PR, Beyssac O (2014) Graphitic carbon: From organic matter to graphite: Graphitization. Elements 10:
477 421-426.

478 Castiñeiras P, Villaseca C, Barbero L, Martín Romera C (2008) SHRIMP U-Pb zircon dating of anatexis in high-
479 grade migmatite complexes of Central Spain: implications in the Hercynian evolution of Central Iberia. Int
480 J Earth Sci 98: 1609-1624.

481 Cesare B, Maineri C (1999) Fluid-present anatexis of metapelites at El Joyazo (SE Spain): constraints from
482 Raman spectroscopy of graphite. Contr Mineral Petrol 134: 41-52.

483 Crespo E, Luque J, Fernández-Rodríguez C, Rodas M, Díaz-Azpiroz M, Fernández-Caliani JC, Barrenechea JF
484 (2004) Significance of graphite occurrence in the Aracena Metamorphic Belt, Iberian Massif. Geol Mag
485 141: 687-697.

486 Crespo E, Luque J, Barrenechea JF, Rodas M (2005) Mechanical graphite transport in fault zones and the
487 formation of graphite veins. Mineral Mag 69: 463-470.

488 Crespo E, Luque J. Rodas M, Wada H, Gervilla F (2006a) Graphite-sulfide deposits in Ronda and Beni Bousera
489 peridotites (Spain and Morocco) and the origin of carbon in mantle-derived rocks. Gond Res 9: 279–290.

490 Crespo E, Luque J, Barrenechea FJ, Rodas M (2006b) Influence of grinding on graphite crystallinity from
491 experimental and natural data: implications for graphite thermometry and sample preparation. Mineral Mag
492 70: 697-707.

493 Gálvez ME, Beyssac O, Martinez I, Benzerara K, Chaduteau C, Malvosin B, Malavieille J (2013) Graphite
494 formation by carbonate reduction during subduction. Nature Geoscience 6: 473-477.

495 Grey IE, Li C, Watts, JA (1983). Hydrothermal synthesis of goethite-rutile intergrowth structures and their
496 relationship to pseudorutile American Mineral 68: 981-988Grey IE, Li C (2003) Hidroxylian pseudorutile
497 derived from picroilmenite in the Murray Basin, Southeastern Australia. Mineral Mag 67: 733-747.

498 Herrero MJ, Martín-Pérez A, Alonso-Zarza AM, Gil-Peña I, Meléndez A, Martín García R (2011) Petrography
499 and geochemistry of the magnesites and dolostones of the Ediacaran Ibor Group (635 to 542 Ma), Western
500 Spain: Evidences of their hydrothermal origin. Sedim Geol 240: 71-84.

501 IGME (1995). Exploración del grafito en España. Centro de Documentación IGME, nº 11415, (unpublished
502 document) Madrid.

503 James HL (1966) Chemistry of the iron-rich sedimentary rocks. Data of Geochemistry, Geol Survey Prof Paper
504 440, 66 pp

505 Kretz R (1983) Symbols for rock-forming minerals. Amer Mineral 68: 277-279.

506 Lazzeri M, Barreiro A (2014) Graphitic carbon: carbon-based nanoscience. Elements 10: 447-452.

507 Luque FJ, Rodas M, Barrenechea JM, Galán Huertos E (1992) Yacimientos españoles de grafito. In: García
508 Guinea J, Martínez Frías J (ed) Recursos minerales de España, CSIC, Madrid, 501-524.

509 Luque F.J, Pasteris JD, Wotapenka B, Rodas M, Barrenechea F (1998) Natural fluid-deposited graphite:
510 Mineralogical characteristics and mechanism of formation. Amer J Sci 298: 471-498.

511 Luque FJ, Crespo-Feo E, Barrenechea JF, Ortega L (2012) Carbon isotopes of graphite: Implications on fluid
512 history. Geos Frontiers 3: 197-207.

513 Luque FJ, Huizenga JM, Crespo E, Wada H, Ortega L, Barrenechea JF (2014) Vein graphite deposits: geological
514 setting, origin and economic significance. Miner Deposita 49: 261-277.

515 Martín Parra LM, Gutiérrez Alonso G, Sánchez Carretero R, Contreras López E, Jorquera de Guindos A, Gracia
516 Prieto FJ (2009) Mapa Geológico de España a escala 1:50.000, hoja nº 656 (Gálvez), IGME, Madrid.

517 Manning CE, Shock EL, Sverjensky DA (2013) The chemistry of carbon in aqueous fluids at crustal and upper-
518 mantle conditions: experimental and theoretical constraints. Rev MineralGeochem 75: 109-148.

519 Martín Romera C, Villaseca C, López-García JA, Boiron MC, Barbero L (2001) CO_2-CH_4-N_2 Fluid inclusions in
520 granulite-facies migmatites of hercynian anatectic complexes of central Spain. XVI ECROFI, 287-289.

521 Nair AG, Suresh Babu DS, Domodaran KT, Shankar R, Prabhu CN (2009) Weathering of ilmenite from Chavara
522 deposit and its comparison with Manavalakurichi placer ilmenite, southwestern India. J Asian Earth Sci 34:
523 115-122.

524 Nakamura Y, Ooashi K, Toyoshima T, Satish-Kumar M, Akai J (2014) Strain-induced amorphization of graphite
525 in fault zones of the Hidaka metamorphic belt, Hokkaido, Japan. J Struct Geol doi:
526 10.1016/j.jsg.2014.10.012

527 Orejana D, Villaseca C, Armstrom RA, Jeffries TE (2010) Geochronology and trace element chemistry of zircon
528 and garnet from granulite xenoliths: Constraints on the tectonothermal evolution of the lower crust under
529 central Spain. Lithos 124: 103-116.

530 Pasteris JD (1989) *In Situ* Analysis in Geological Thin-Sections by Laser Raman Microprobe Spectroscopy: A
531 Cautionary Note. Applied Spectroscoy 43: 567-570

532 Pasteris JD, Wopenka B (1991) Raman spectra of graphite as indicators of degree of metamorphism. Canadian
533 Mineralogist 29: 1-9.

534 Peters D (2011) Mineralogical and chemical characterization of alunita group minerals from hydrothermal veins
535 of the Sultana mineralization/SE Spain. Dissertation, Johanes Gutenber-University Mainz, Institute of
536 Geosciences.

537 Pimienta MA, Dresselhaus G, Dresselhaus MS, Cançado LG, Jorio A, Saito R (2007) Studying disorder in
538 graphite-based systems by Raman spectroscopy. Phys Chem Chem Physics 9: 1276-1291.

539 Rodas M, Luque FJ, Barrenechea JF, Fernández-Caliani JC, Miras A, Fernández-Rodríguez C (2000). Graphite
540 occurrences in the low-pressure/high-temperature metamorphic belt of Sierra de Aracena (southern Iberian
541 Massif). Mineralogical Magazine 64: 801-814

542 Rumble D (2014) Hydrothermal graphitic carbon. Elements 10: 427-433.

543 Sánchez Carretero R, Contreras López E, Martín Parra L, Martínez-Salanova J, Gutiérrez Alonso G, Barbero L,
544 Villaseca C (2009) Mapa geológico de España 1: 50 000, hoja nº 657 (Sonseca), IGME, Madrid

Sánchez Ronda D (2013) Una aproximación a las nuevas formas alotrópicas del carbono y al beneficio del grafito en la provincia de Toledo. Graduate Dissertation, Universidad Politécnica, Almadén. 224 pp.

Sanyal P, Acharya BC, Bhattacharya SK, Sarkar A, Agrawal S, Bera MK (2009) Origin of graphite, and temperature of metamorphism in Precambrian Eastern Ghats Mobile Belt, Orissa, India: A carbon isotope approach. J Asian Earth Sci 36: 252-260.

Scherrer P (1918) Bestimmung der grösse un der inneren struktur von kolloidteilchen mittels Röngntgenstrahlen, nachrichten von der gesellschaft der wissenschaften, Göttingen Mathem Physik Klasse 2: 98-100.

Shengelia DM, Akhvlediani RA, Ketskhoveli DN (1979) The graphite geothermometer. Dobkl. Acad. Nauk. USSR 235: 132-134.

Spear FS (1993) Metamorphic Phase Equilibria and Pressure-Temperature-Time Paths. Mineralogical Society of America Monograph, Washington.

Touzain P, Balasooriya N, Bandaranayake K, Descolas-Gros C (2010) Vein graphite from the Bogala and Kahatacha-Kolongaha Mines, Sri-Lanka: A possible origin. Canad Mineral 48: 1373-1384.

Villaseca C, Downes H, Pin C, Barbero L (1999) Nature and composition of the lower continental crust in Central Spain and the granulite-granite linkage: interferences from granulitic xenoliths. J Petrol 40: 1465-1496.

Villaseca C, Merino E, Oyarzun R, Orejana D, Pérez-Soba C, Chicharro E (2014) Contrasting chemical and isotopic signatures from Neoproterozoic metasediments in the Central-Iberian Zone of pre-Variscan Europe (Spain): implications for terrane analysis and early Ordovician magmatic belts. Precam Res 245: 131-145.

Wada H (1988) Microscale isotopic zoning in calcite and graphite crystals in marble. Nature 331: 61-63.

Wopenka B, Pasteris JD (1993) Structural characterization of kerogens to granulite-facies graphite: Applicability of Raman microprobe spectroscopy. Amer Mineral 78: 533-557.

Key to Figures

Figure 1 – Geological map of the ACT (based on Barbero 19992; Barbero and Villaseca 2004; Martín Parra et al. 2009; Sánchez-Carretero et al. 2009). To the south of the Toledo shear band outcrop late-Variscan granites and Paleozoic and Neoproterozoic metasedimentary sequences most of them included in the Schist-Greywacke Formation (SGF) from the southern Central Iberian Zone (see Villaseca et al. 2014, and references therein).

Figure 2 – Occurrences of graphite-bearing rocks in La Puebla de Montalbán mine site. (a) Parallel late shear micro bands with local concentration of graphite, in a mining pit (samples 114554, 114555 and 114556). (b) Micro shears affecting a graphite-rich granulite (sample 114568).

Figure 3 – BSE microphotographs illustrating graphite textures. Guadamur site: (a) Graphite prisms within granulitic minerals (sillimanite, quartz, ilmenite) (sample 114423). (b) Photomicrograph taken under plane-polarized light. Graphite flakes within quartz in granulite (sample 114400). (c) Graphite within muscovite and sericitized plagioclase, with accessory ilmenite (sample 114434). (d) Graphite within muscovite, chlorite, and associated goethite (sample 114431). (e) Graphite within kaolinite and numerous rounded goethite crystals in the upper left quadrant (sample 114432). (f) Tailing rock with jarosite- and goethite-banding, showing interstitial micropholded grphite (sample 114432). (g) Microfolded graphite with associated goethite-chamosite in a calcite-bearing breccia (sample 114427). (h) Calcite veins within altered graphite-bearing rock (sample 114635). (i) Calcite veins with accessory aragonite in vugs (geodes) (sample 114635). La Puebla de Montalbán site: (j) Graphite flakes interstitial to pseudorutile, quartz and K-feldspar crystals (granulite sample 114568). Symbols: Gr= graphite, Sil= sillimanite, Ilm= ilmenite, Qtz= quartz, Ms= muscovite, Pl= plagioclase, Chl=chlorite, Gt= goethite, Kln= kaolinite, Jar= jarosite, Chm= chamosite, Cal= calcite, Arg= aragonite, Psrt= pseudorutile, Kf= K-feldspar (after Kretz 1983).

Figure 4 – Examples of Raman spectra of the well-ordered ACT graphite. (a) Spectra of high R1 and R2 Raman parameters (sample 114568 from La Puebla de Montalbán), (b) Spectra of highly crystalline graphite in a highly retrograded sample form the Guadamur mine site (tailing 114432)

Figure 5 – Histogram plot of the graphite $\delta^{13}C$ composition from the ACT. The carbon isotope data show three isotopic groups of biogenic carbon sources.

Figure 6 – Summary of *P-T* conditions of graphite-bearing rocks from the ACT plotted together averaged P-T estimates of the high-grade conditions of the ACT from Barbero (1992, 1995). Estimates for CO_2-rich fluid inclusions (FI) taken from Martín Romera et al. (2001). Petrogenetic grid for phyllosilicates in pelitic rocks is taken from Spear (1993).

Figure 7 – Relationships between stable carbon isotope results and estimated temperature of retrogradation of graphite-bearing rocks in the mining sites of the ACT. Averaged P-T estimates of the high-grade conditions of the ACT from Barbero (1992, 1995), and for sample U-10 from the lower crust of central Spain, from Villaseca et al. (1999). Carbon isotope data from dolostones of the Schist Greywacke Complex (with $\delta^{13}C$ from -4.4 to +3.2 ‰) is taken from Herrero et al. (2011) and biogenic sources (including hydrothermal H_2O-NH_4-rich fluids) is taken from Luque et al. (2012).

Key to Tables

Table 1 – Representative mineral composition (EMP data) of the ACT samples

Table 2 – Summary of chemical and structural (XRD and Raman spectroscopy) features of graphite in the ACT

Table 1

Table 1. Representative mineral composition (EPMA data) of the ACT samples

Mineral	Bt	Ms	Ms	Ms	Ms	Ms	Chl	Chl	Kln	Gt	Chm	Jar	Ilm	Ant	Ps-Rt	Ps-Rt	HSR	HSR
Sample	114570	114429	114434	114431	114557	114638	114431	114635	114432	114432	114427	114432	114434	114434	114568	114568	114569	114569
Location	Granulite Montalbán	Guadamur mine	Guadamur mine	Guadamur mine	Montalbán mine	Montalbán mine	Guadamur mine	Guadamur mine	Guadamur mine	Guadamur mine	Guadamur mine	Guadamur mine	Guadamur mine	Guadamur mine	Granulite Montalbán	Granulite Montalbán	Montalbán mine	Montalbán mine
Analysis	14.2	12.1	28.1	32.1	19.2	35.2	35.1	28.2	21.1	24.1	40.1	18.1	30.1	31.1	9.2	10.2	1.2	6.2
SiO_2	34.73	45.72	44.38	44.83	45.13	45.32	26.32	25.60	46.08	1.64	20.26	1.15	1.38	0.28	0.50	2.38	1.91	5.72
TiO_2	4.83	0.09	0.11	0.23	0.38	0.02		0.22	0.02			0.02	55.20	93.45	61.30	59.09	75.09	74.56
Al_2O_3	18.57	35.62	35.01	33.14	35.83	36.41	22.48	21.30	37.55	3.33	10.75	4.05	0.84	0.40	0.93	1.52		4.93
FeO	19.80	1.33	1.43	2.04	0.10	0.69	25.01	25.85	0.51	69.95	44.30	36.51	35.31	3.70	29.24	27.89	13.61	8.33
MnO	0.07	0.05			0.01	0.02	0.17	0.06	0.01	0.11	0.03		0.92		0.09	0.04	0.01	0.04
MgO	7.32	0.05	0.67	1.03	0.32	0.09	11.51	10.35	0.05		1.02	0.01	0.09		0.25	0.27		1.21
CaO		0.03	0.04	0.01	0.11	0.02	0.38	0.09	0.12	0.31	0.85	0.06	0.05	0.12	0.53	0.60		0.54
Na_2O	0.19	0.27	0.59	0.62	0.62	0.43		0.01	0.03	0.06	0.02	0.07	0.04	0.02	0.01	0.01		0.02
K_2O	8.89	9.86	10.08	9.54	10.14	9.92	0.30	0.15	0.04	0.03	0.81	8.20	0.12	0.03				
P_2O_5	0.01						0.01			1.68	0.52	0.02	0.03	0.07	0.18	0.18	0.03	0.02
ZnO										0.12	0.19		0.69	0.08				
Cr_2O_3	0.12							0.29							0.08	0.13	0.05	0.07
SO_3										0.56	0.11	29.31		0.05	0.01		0.01	
Total	94.75	93.09	92.46	91.60	93.58	92.92	86.90	84.00	84.49	77.82	78.89	79.77	94.51	98.18	93.37	92.49	90.95	95.71

Mineral abbrevations: Bt = biotite, Ms = muscovite, Chl = chlorite, Kln = kaolinite, Gt = goethite, Chm = chamosite, Jar = jarosite, Ilm = ilmenite, Ant = anatase, Ps-Rt = pseudorutile, HSR = hydroxylated pseudorutile, mostly after Kretz (1983). Blank rows are data below detection limits.

Table 2

Table 2 - Summary of isotopic and structural (XRD and Raman spectroscopy) features of graphite in the ACT

Sample	Locality	Lithology	Mineral association	Alteration intensity	$\delta^{13}C$ (‰)	± 1σ	graphite (%)	XRD results				Raman results			
								2θ	d(002) (A)	FWHM (2θ)	Lc (002) (A)	G position	G-FWHM (cm^{-1})	R1	R2
			High-T rocks												
U-10	SCS lower crust	Granulite	Qtz-Grt-Sil-Pl-Rt	-	-18.28	0.29									
U-10	SCS lower crust	Granulite	Qtz-Grt-Sil-Pl-Rt	-	-19.70	0.19	0.5*	26.56	3.354	n.d.		1580	15.33	0.04	0.11
114400	Guadamur	Granulite	Qtz-Pl-Bt-Grt-Ilm	-	-20.59	0.09	0.2*	26.55	3.354	n.d.		1580	16.46	0.05	0.12
114632	Guadamur	Granulite	Sil-Qtz-Ilm-Alt	med	-27.76	0.07	23.5*								
114633	Guadamur	Granulite	Qtz-(Pl-Kf)-Bt-Grt-Sil-Ilm	med	-20.92	0.01	21.2*								
114568	P. Montalbán mine	Sheared granulite	Qtz-Pl-Kf-Bt-Sil-Grt-(Crd)-Ilm	low	-20.91	0.06	9.5*	26.47	3.365	0.104	820	1580	18.64	0.12	0.22
114571	Puebla Montalbán	Granulite	Qtz-Pl-Kf-Bt-Sil-Grt-(Crd)-Ilm	med	-23.38	0.03	20.1*	26.48	3.363	0.076	1120	1581	16.34	0.03	0.08
114566	Puebla Montalbán	Granulite	Qtz-Crd-Kf-Sil-Pl-Bt-Grt-Ilm	-	-20.58	0.16	2.8*								
114567	Puebla Montalbán	Granulite	Qtz-Pl-Kf-Bt-Sil-Grt-(Crd)-Ilm	low	-20.46	0.06	1.5*								
			Mid-to-low-T rocks												
114428	Guadamur mine site	Retrograded rock	Qtz-Pl-Ms-Chm-Alt	high	-27.63	0.12	12.3	26.52	3.359	0.085	1000	1579	15.06	0.00	0.03
114429	Guadamur mine site	Retrograded rock	Qtz-Pl-Ms-Chm-Gt-Alt	high	-27.86	0.03	10.2	26.50	3.362	0.089	958	1580	14.64	0.02	0.05
114430	Guadamur mine site	Retrograded rock	Qtz-Pl-Ms-Chm-Gt-Cal-Alt	high	-27.86	0.12	10.0	26.52	3.358	0.082	1040				
114431	Guadamur mine (trench)	Retrograded rock	Qtz-(Bt)-Ms-Chl-Alt	med	-27.64	0.06	7.6								
114432	Guadamur mine (waste)	Retrograded (supergenic)	Qtz-Kln-Gt-Jar-Alt	high	-27.78	0.04	7.8	26.50	3.360	0.071	1200	1580	15.83	0.02	0.05
114433	Guadamur mine (waste)	Retrograded (supergenic)	Qtz-Prl-Alt	high	-27.75	0.19	7.0	26.50	3.360	0.090	948	1579	16.07	0.02	0.05
114434	Guadamur mine (waste)	Retrograded rock	Qtz-Ms-Ilm-Gt-Alt	high	-27.59	0.06	24.7	26.48	3.363	0.097	879	1581	16.07	0.10	0.05
			Mid-T deformed rocks												
114554	P. Montalbán mine	Cataclasite	Qtz-(Bt)-Pl-Alt	med	-23.15	0.02	2.2	26.49	3.362	0.103	828				
114555	P. Montalbán mine	Milonite	Qtz-Ms-(Pl)-Cal-Alt	high	-23.03	0.30	4.4	26.50	3.361	0.082	1040				
114556	P. Montalbán mine	Cataclasite	Qtz-Ms-(Bt)-(Pl)-Alt	med	-23.13	0.16	3.1	26.50	3.361	n.d.		1579	18.17	0.06	0.15
114557	P. Montalbán mine	Cataclasite	Qtz-Ms-Cal-Alt	high	-23.01	0.24	5.8	26.45	3.367	0.106	805	1579	14.79	0.01	0.02
114558	P. Montalbán mine	Milonite	Qtz-Ms-(Bt)-(Pl)-(Grt)-Cal-Alt	med			7.8	26.54	3.359	n.d.		1579	16.83	0.03	0.10
114635	Guadamur mine	Hydrothermal vein	Cal	high	-5.15	0.001									

Mineral abbrevations: Qtz = quartz, Grt= garnet, Sil= sillimanite, Pl= plagioclase, Rt= rutile, Bt= biotite, Ilm= ilmenite, Kf= k-feldspar, Crd= cordierite, Ms= muscovite, Chm= chamosite, Gt= goethite, Cal= calcite, Chl= chlorite, Kln= kaolinite, Jar= jarosite, Prl= Pyrophilite, mostly after Kretz (1983). Alt= clay minerals; Alteration intensity: - (null), low (< 10%, mainly feldspars), medium (10-50%, feldspars, cordierite, biotite), high (> 50% supergenic minerals). * = based in modal estimation

Figure 1

Click here to download Figure Figura 1 Colour.tif

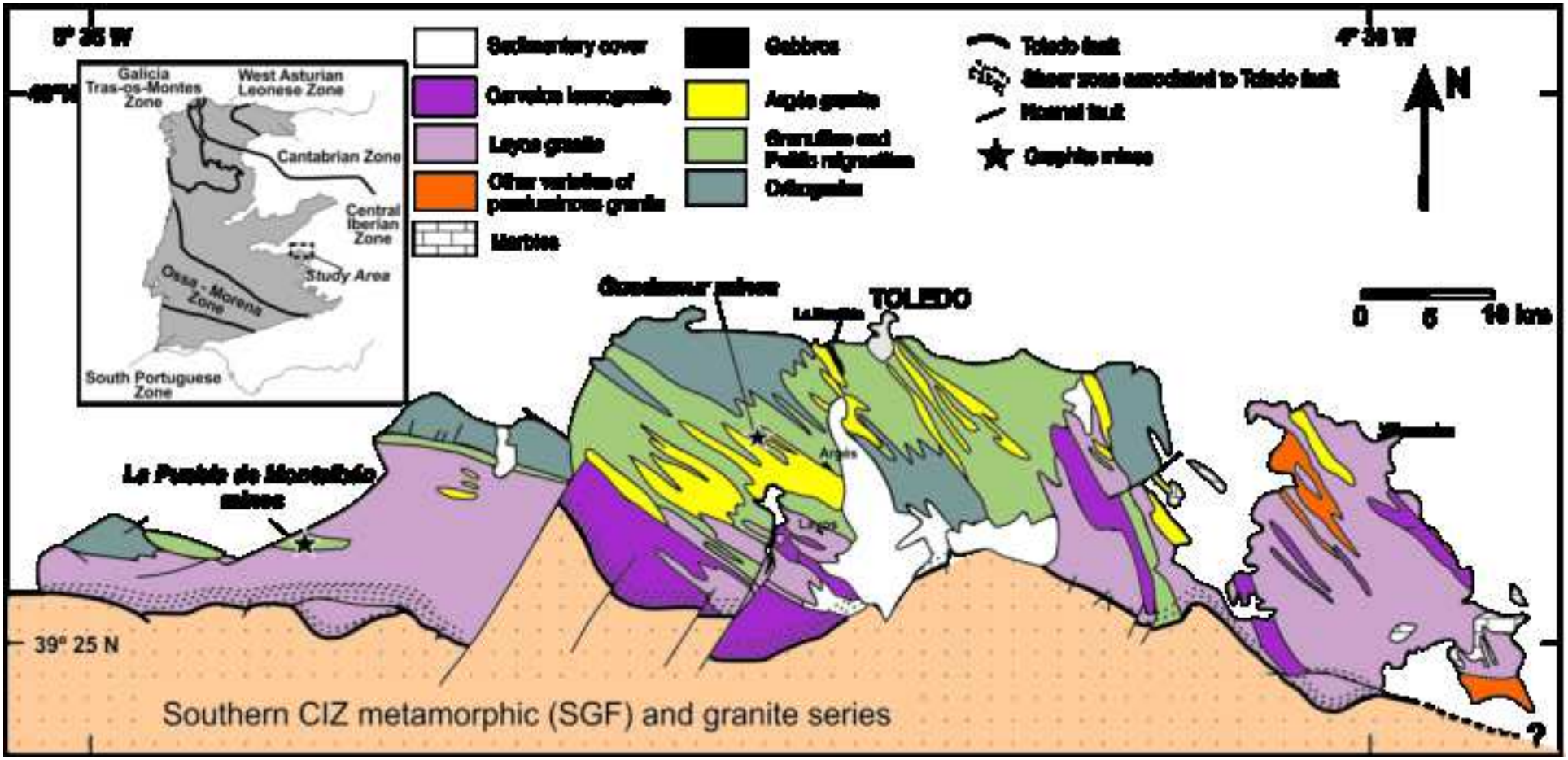

Figure 2

Click here to download Figure Figura 2.tif

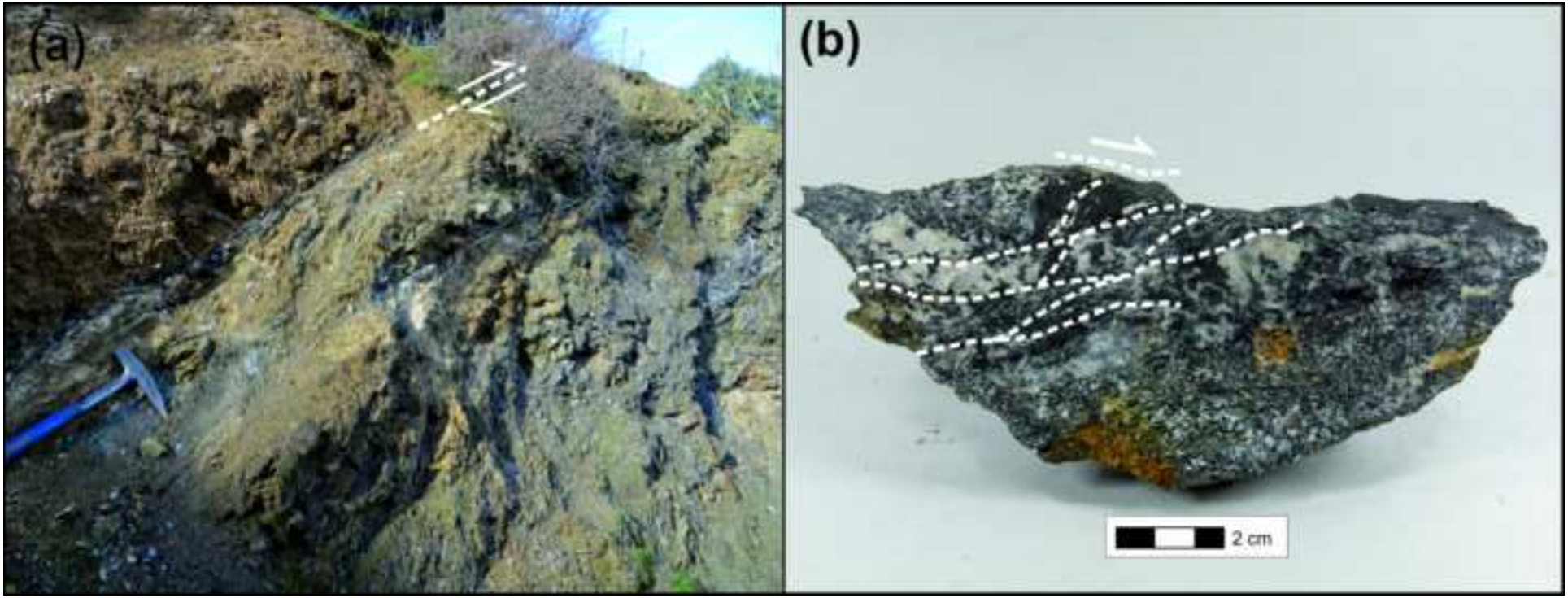

Figure 3 (I)

Click here to download Figure Figura 3 Esquema de fotos (I).tif

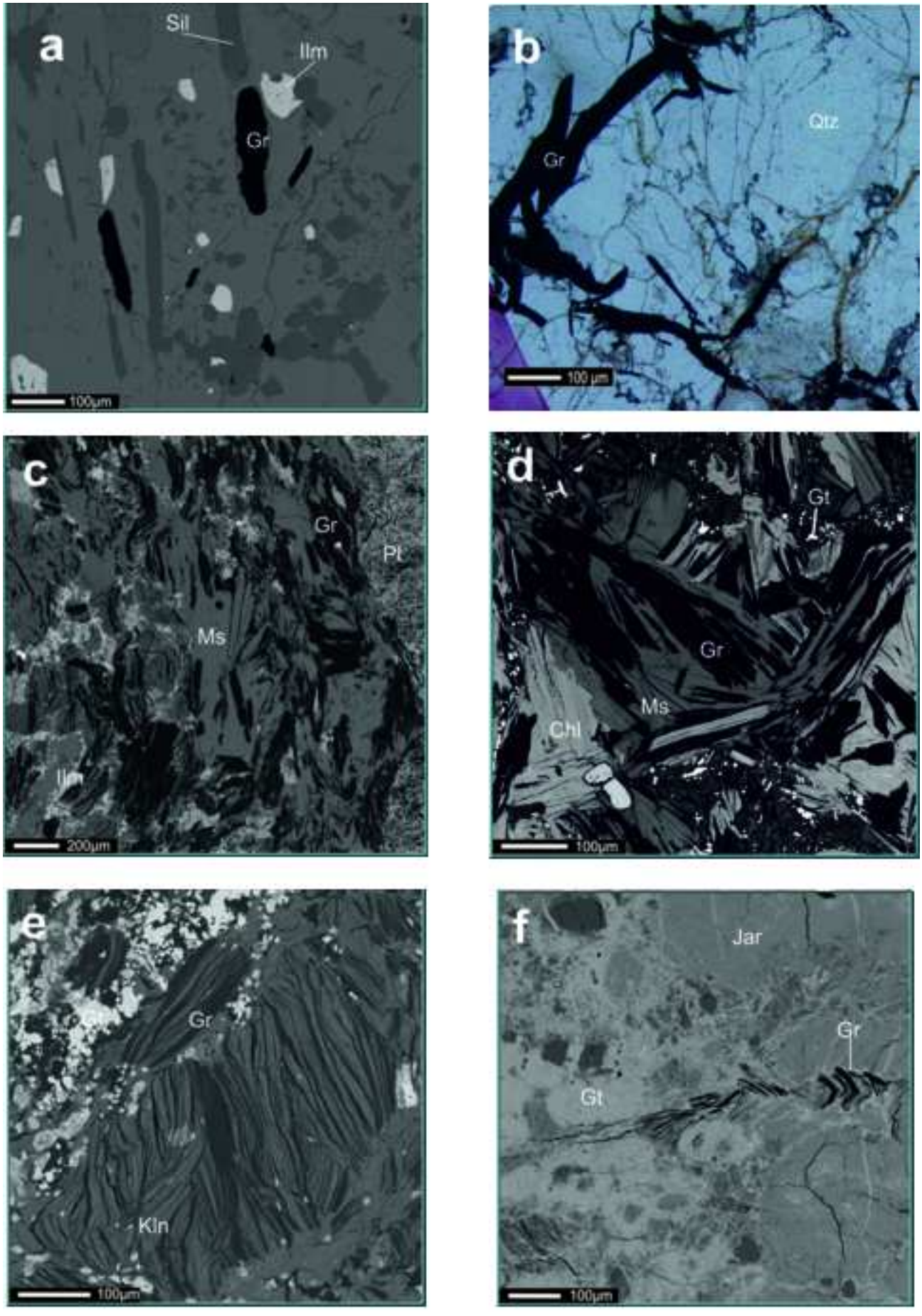

Figure 3 (II)

Click here to download Figure Figura 3 Esquema de fotos (II).tif

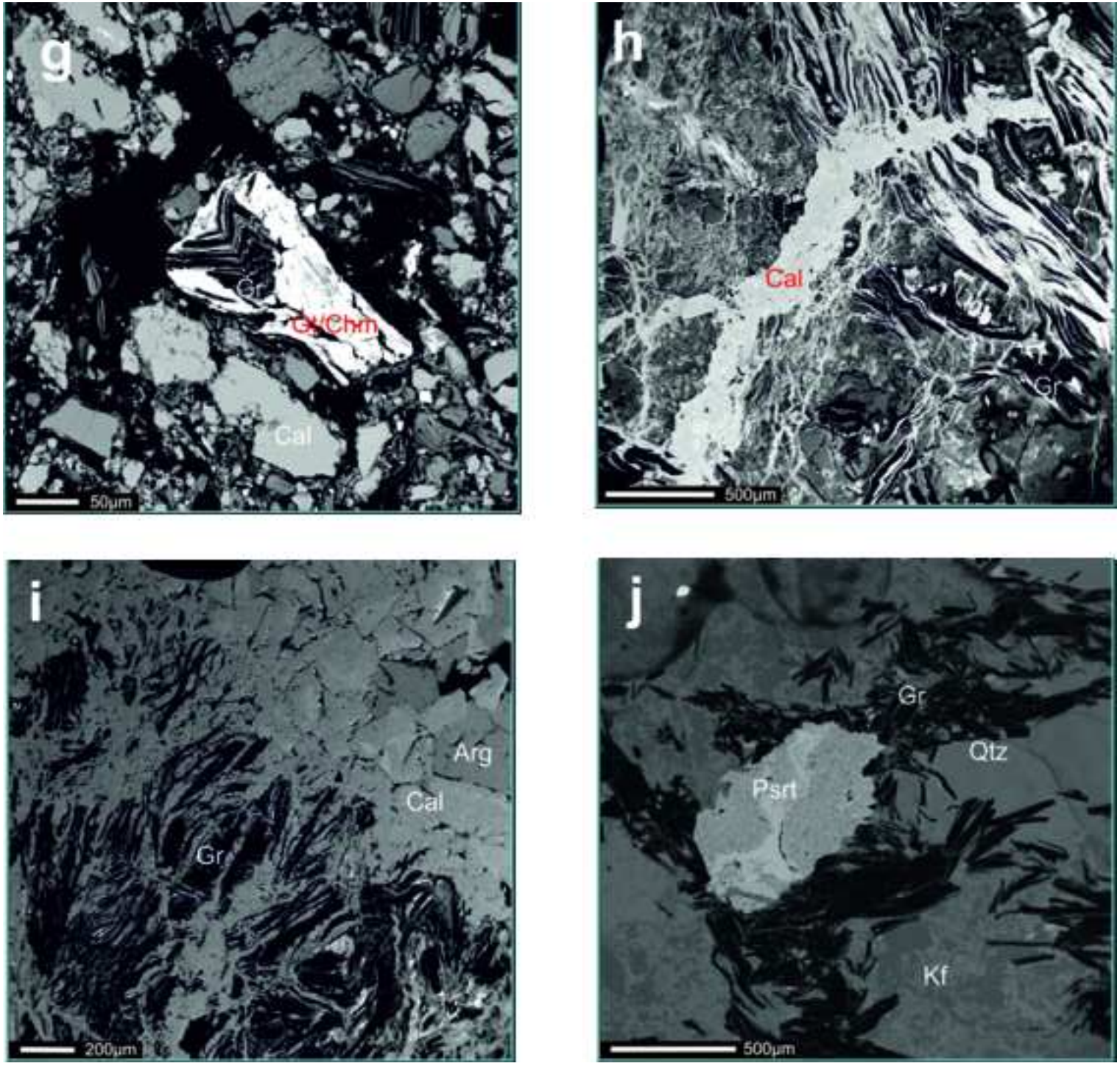

Figure 4

Click here to download Figure Figure 4.tif

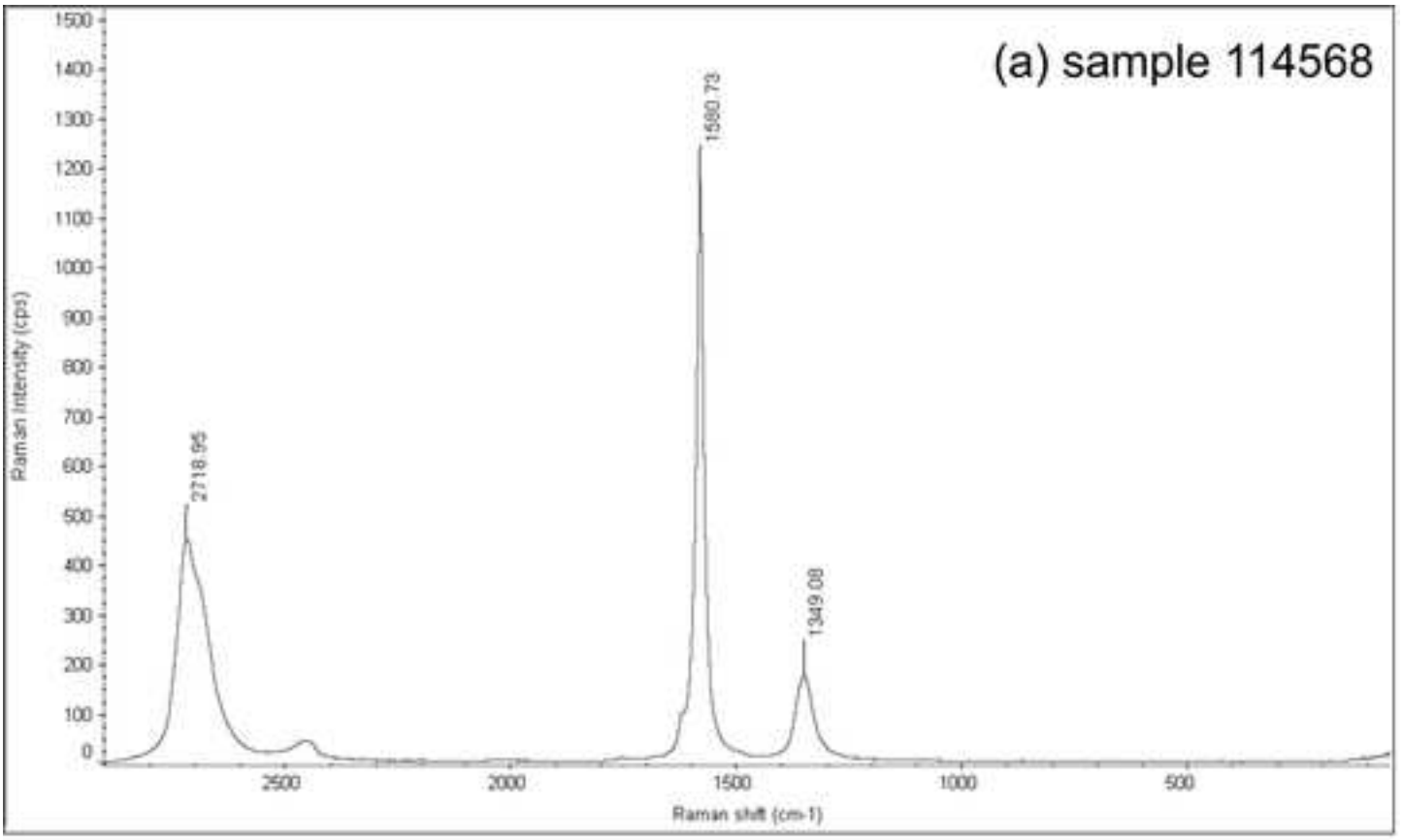

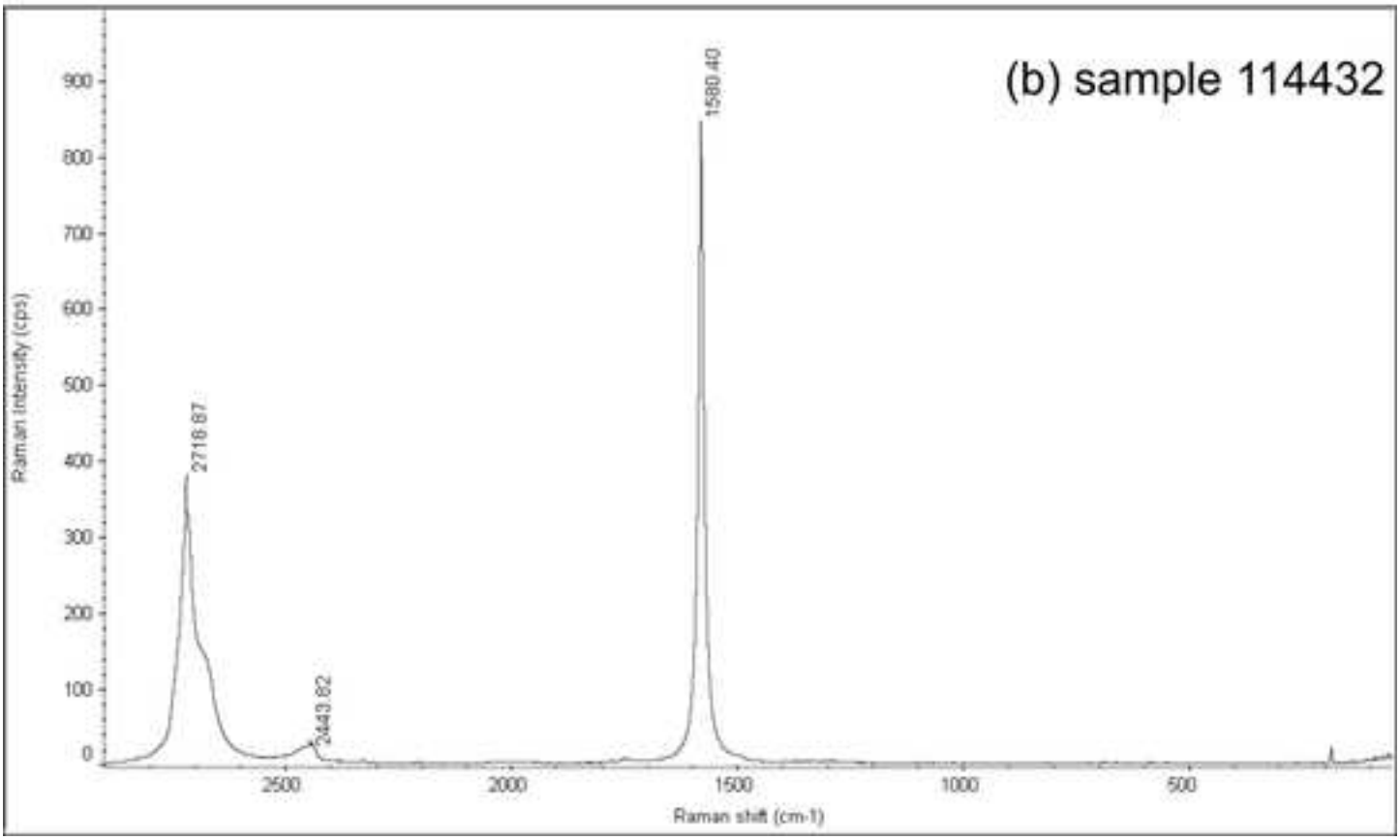

Figure 5

Click here to download Figure Figura 5.tif

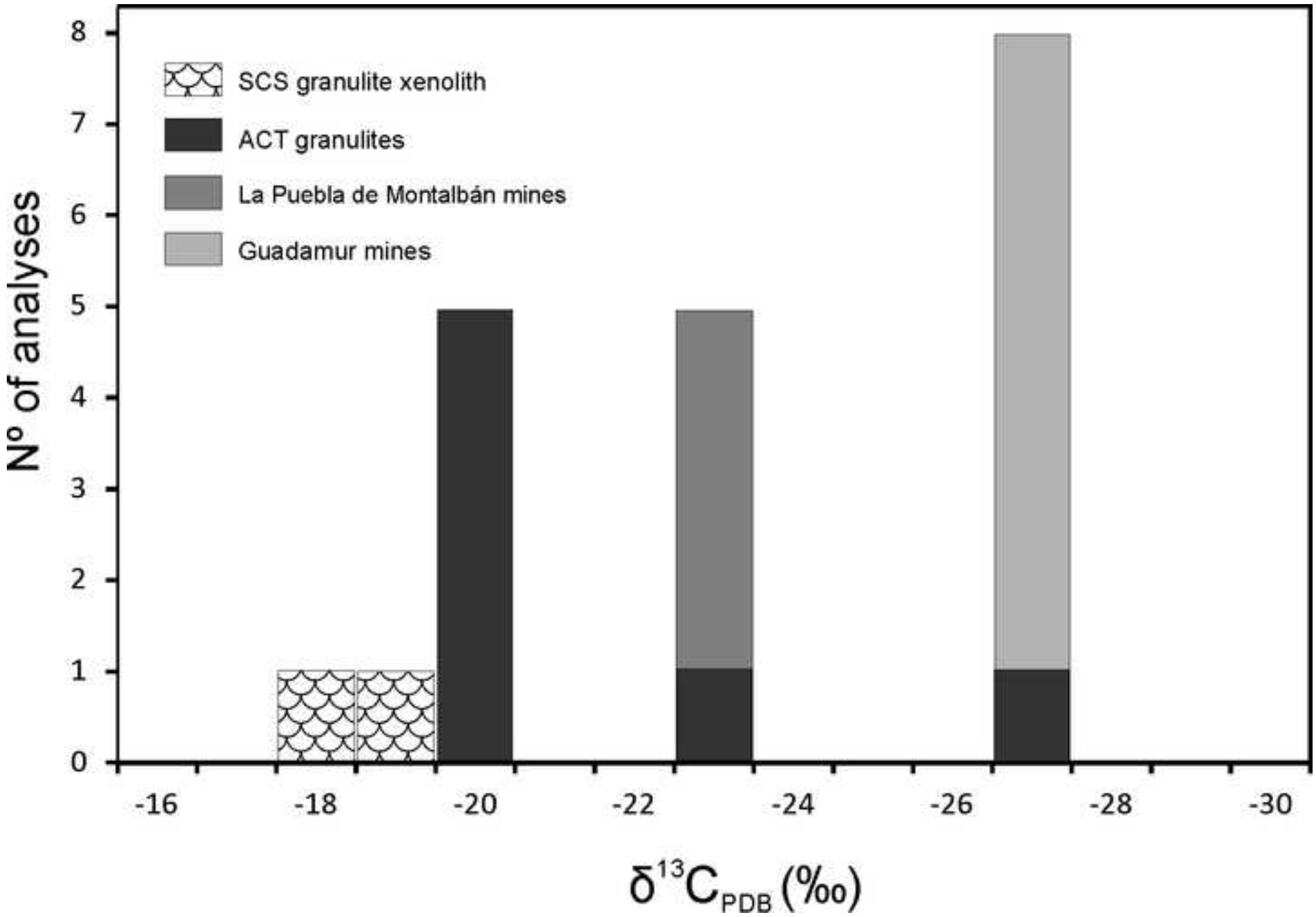

Figure 6

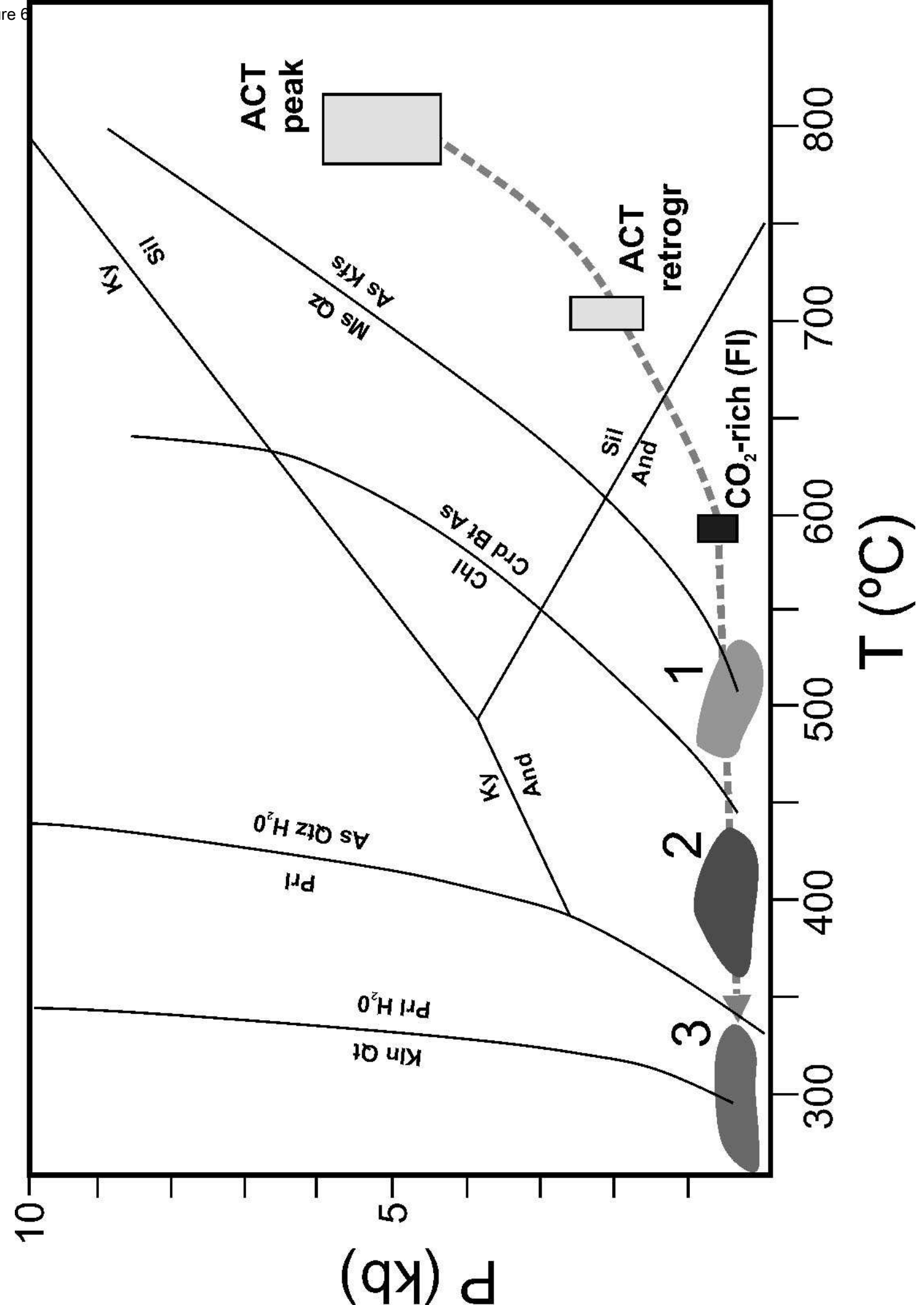
ACT peak
ACT retrogr
CO2-rich (FI)
Ms Qz As Kfs
Ky Sil
Chl Crd Bt As
Sil And
Ky And
As Qtz H2O
Prl
Prl H2O
Kln Qt
1
2
3
P (kb)
T (°C)
10
5
300
400
500
600
700
800

Figure 7

Click here to download Figure Figura 7.tif